Magnetic Reconnection between Colliding Magnetized Laser-Produced Plasma Plumes

G. Fiksel, W. Fox, A. Bhattacharjee, D. H. Barnak, P.-Y. Chang, K. Germaschewski, S. X. Hu, and P. M. Nilson

Phys. Rev. Lett. **113**, 105003 — Published 4 September 2014
DOI: 10.1103/PhysRevLett.113.105003

Magnetic reconnection between colliding magnetized, laser-produced plasma plumes

G. Fiksel[1,2],* W. Fox[3], A. Bhattacharjee[3], D.H. Barnak[1,2], P.-Y. Chang[1,2], K. Germaschewski[4], S.X. Hu[1], and P.M. Nilson[1,2]
[1]*Laboratory for Laser Energetics, University of Rochester, Rochester, NY 14623*
[2]*Fusion Science Center for Extreme States of Matter, University of Rochester, Rochester, NY 14623*
[3]*Department of Astrophysical Sciences and Princeton Plasma Physics Laboratory, Princeton, NJ 08543*
[4]*Space Science Center, University of New Hampshire, Durham, NH, 03824*
(Dated: August 12, 2014)

Observations of magnetic reconnection between colliding plumes of magnetized laser-produced plasma are presented. Two counter-propagating plasma flows are created by irradiating oppositely placed plastic (CH) targets with 1.8-kJ, 2-ns laser beams on the Omega EP Laser System. The interaction region between the plumes is pre-filled with a low-density background plasma and magnetized by an externally applied magnetic field, imposed perpendicular to the plasma flow, and initialized with an X-type null point geometry with $B = 0$ at the midplane and $B = 8\,\mathrm{T}$ at the targets. The counter-flowing plumes sweep up and compress the background plasma and the magnetic field into a pair of magnetized ribbons, which collide, stagnate, and reconnect at the midplane, allowing the first detailed observations of a stretched current sheet in laser-driven reconnection experiments. The dynamics of current sheet formation are in good agreement with first-principles particle-in-cell simulations that model the experiments.

PACS numbers: 52.27.-h, 52.35.Vd, 52.65.Rr, 52.72.+v, 94.30.cp

Throughout the Universe, magnetic reconnection allows the magnetic field to change its topology and thereby allow an explosive release of stored energy [1–3]. Recently, a number of experiments have been carried out studying magnetic reconnection using laser-driven plasmas [4–8]. These experiments are in many ways complementary to traditional reconnection experiments with magnetized discharge plasmas [3]. Some notable features include the high plasma beta, strong inflows, and strong magnetic flux pile-up. This regime is very interesting as there are a number of space and astrophysical contexts where supersonic, magnetized flows collide, such as interactions of planetary magnetospheres with the solar wind [9], interaction of the solar wind with the interstellar medium at the heliopause [10, 11], and pulsar wind-termination shocks [12], to name only a few.

Previous laser-driven experiments studied the reconnection of the self-generated (e.g., Biermann battery) magnetic fields between colliding laser-produced plasma plumes [4–8]. Magnetic field annihilation [5] has been observed, as well as plasma jets [4, 6–8] and electron energization [8]. This Letter presents, for the first time, results on reconnection of an *externally applied* magnetic field by counter-propagating, laser-driven colliding high-energy density (HED) plasmas. These experiments are based on new techniques for externally controlled magnetization of ablated plasma plumes. The geometry of this externally magnetized plasma experiment makes it amenable to end-to-end simulation with particle-in-cell codes modeling the entire progression of the experiment, including plasma formation and assembly of the current sheet. While previous results in HED plasmas could infer reconnection through annihilation of the magnetic field [5], this work is the first to observe clear stagnation of the counter-propagating magnetized ribbons and the formation of an extended reconnection layer. The reconnection layer stagnates at a width comparable to the ion skin depth and shows the formation of cellular structures that may indicate the formation of magnetic islands or plasmoids. The magnetic fields in the current sheet are observed to suddenly and completely annihilate, an effect not yet captured in our two-dimensional (2-D) simulation.

The experiment was carried out on the Omega EP Laser System [13] at the University of Rochester. Figure 1 shows the experimental setup. Two counter-propagating *drive* plasma plumes were obtained by irradiating oppositely placed plastic (CH), $2 \times 6 \times 0.25\,\mathrm{mm}^3$ ablator targets with two 1.8-kJ, 2-ns laser beams (drive beams) at a wavelength of $0.351\,\mu\mathrm{m}$ and on-target laser intensities of $5 \times 10^{13}\,\mathrm{W/cm}^2$. The targets were separated by 4.25 mm and the laser beam incidence angle of 74° resulted in highly elliptical, $1 \times 3\,\mathrm{mm}^2$ focal spots. The highly elongated focal footprint shape conforms to a quasi-2-D geometry, making it suitable for comparison with 2-D simulations.

An external magnetic field, imposed perpendicular to the plasma flow, was created by current-carrying conductors placed directly behind each target and powered by MIFEDS (Magneto-Inertial Fusion Electrical Discharge System) [14]. The current pulse had a duration of $1\,\mu\mathrm{s}$ and the drive lasers were fired at the peak of the magnetic field. Two parallel currents (into the page in Fig. 1) were used to impose a field with an X-type null point and field reversal between the colliding plasmas–a typical reconnection geometry [1, 3]. The magnetic field profile was $B = 0$ at the midplane and monotonically increased to $B = 8\,\mathrm{T}$ at the targets. The pre-imposed (vacuum)

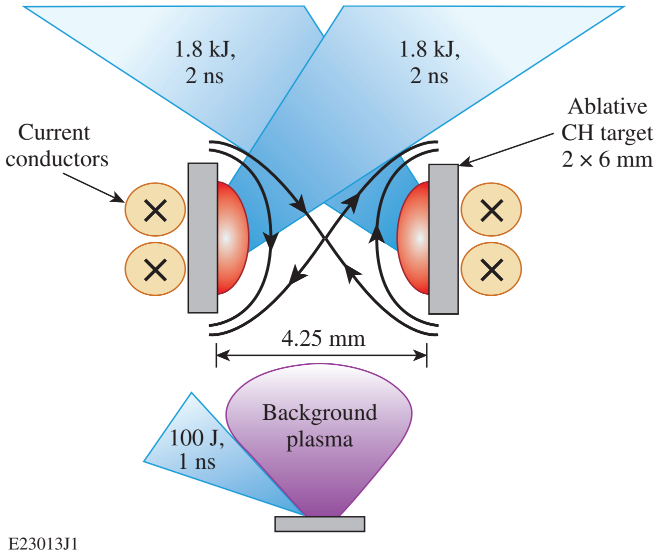

FIG. 1. (Color online). Experimental setup. Two counter-propagating drive plasma plumes are obtained by irradiating two opposing plastic (CH) ablator targets. An external magnetic field was created by pulsing an electric current through conductors located directly behind each target. The region between the ablator targets was pre-filled by a tenuous background plasma created by a dedicated laser-ablator pair. A multi-MeV proton beam (not shown) generated with a high-intensity short-pulse laser beam was used to probe the dynamics and topology of the magnetic field in the interaction region.

magnetic flux ($\int B_z dx$ from foil to X-point) available for reconnection is approximately 8×10^{-3} Tm. In the process of the plumes colliding and merging, the magnetic field is expected to be first compressed into a current sheet, accompanied by reconnection.

The X-point region between the ablators was pre-filled by a tenuous *background* plasma created by ablating a third target ($2 \times 2 \times 0.25\,\mathrm{mm}^3$ and 5 mm from the x-point) with a third laser pulse (100 J, 1 ns), fired 12 ns before the main drive beams to give the plume enough time to pre-fill the interaction volume. The purpose of the background plasma is to embed or thread the magnetic field prior to being compressed by the drive plasma. Experiments without a background plasma did not show reconnection, a fact that will be discussed in more detail below.

The dynamics and topology of the magnetic field in the interaction region were probed with proton radiography [15]. This diagnostic used an ultrafast proton beam generated with a high-intensity, short-pulse laser beam ($1.053\,\mu$m/800 J/10 ps) focused to a 25-μm spot on a thin 20-μm copper foil. The protons, accelerated by the target-normal sheath acceleration (TNSA) mechanism [16], have a broad distribution of energies of the order of 10 MeV and higher. Protons are detected in a stack of radiochromic film (RCF) interleaved with aluminum foils of various thickness. The RCF detector is placed 80 mm from the interaction region, for a geometrical magnification of $M = 11$, with proton energies resolved in the film stack by their respective energy-dependent Bragg peaks. The temporal resolution of the detector is about 100 ps. While passing through the interaction region (inboard in Fig. 1), the protons are focused or defocused by magnetic fields in the magnetized plumes, leaving an intensity pattern at the detector. The temporal evolution of the magnetic field structure was obtained over multiple shots by varying the timing of the proton beam with respect to the drive laser beams.

A series of representative proton radiography images in Fig. 2a—2d illustrate four stages in the magnetic field evolution: (a) formation of magnetic "ribbons" and the sweeping up of background plasma and magnetic field, (b) collision of magnetic ribbons, (c) reconnection, and (d) magnetic field annihilation. The time stamps on each frame show the time when the proton beam fired relative to the drive beams. Distinctive features common to the images are the two light-colored curved bands containing a high magnetic field, described here as magnetic ribbons. The direction of the vertical component of the magnetic field, upward on the right ribbon and downward on the left ribbon (Fig. 1), is such that the diagnostic protons are deflected outward from each corresponding ribbon. The magnetic field in the ribbons is strong enough to completely deflect the protons from those regions, leaving a deficit of protons and reflected as white, unexposed film. A sharp, "caustic" proton boundary [17] of very high fluence - a feature well-reproduced in our modeling– appears immediately on the outside of each ribbon, forming an important point of comparison between simulation and experiment.

During the plume expansion stage (Fig. 2a) the shape of the ribbons is topologically equivalent to the shape of the vacuum magnetic field lines. At $t = 2.37$ ns, each ribbon has traversed more than halfway to the midplane. The magnetic field in each ribbon has been strongly compressed above the vacuum field as indicated by a low proton fluence in the ribbons. This stage is a clear manifestation of the initial magnetic field being swept up by the high-pressure plasma plumes, as would be expected by the high plasma pressure compared to the magnetic field pressure. The degree of field compression by the pileup can be estimated by assuming that all of the initially available flux $\Phi \approx 8$ T mm is compressed into a ribbon with a thickness of $\delta \approx 0.3$ mm, resulting in a compressed field $B_{comp} \approx \Phi/\delta \approx 25$ T.

At $t = 3.12$ ns, (Fig. 2b), the ribbons collide and flatten out. The magnetic field in the collision region is strongly compressed, expelling virtually all the fast protons. The ribbon width stagnates, indicating stagnation of the plasma flow. Based on the opposing signs of the incoming magnetic fields, the collision of the ribbons must produce a reconnecting current sheet.

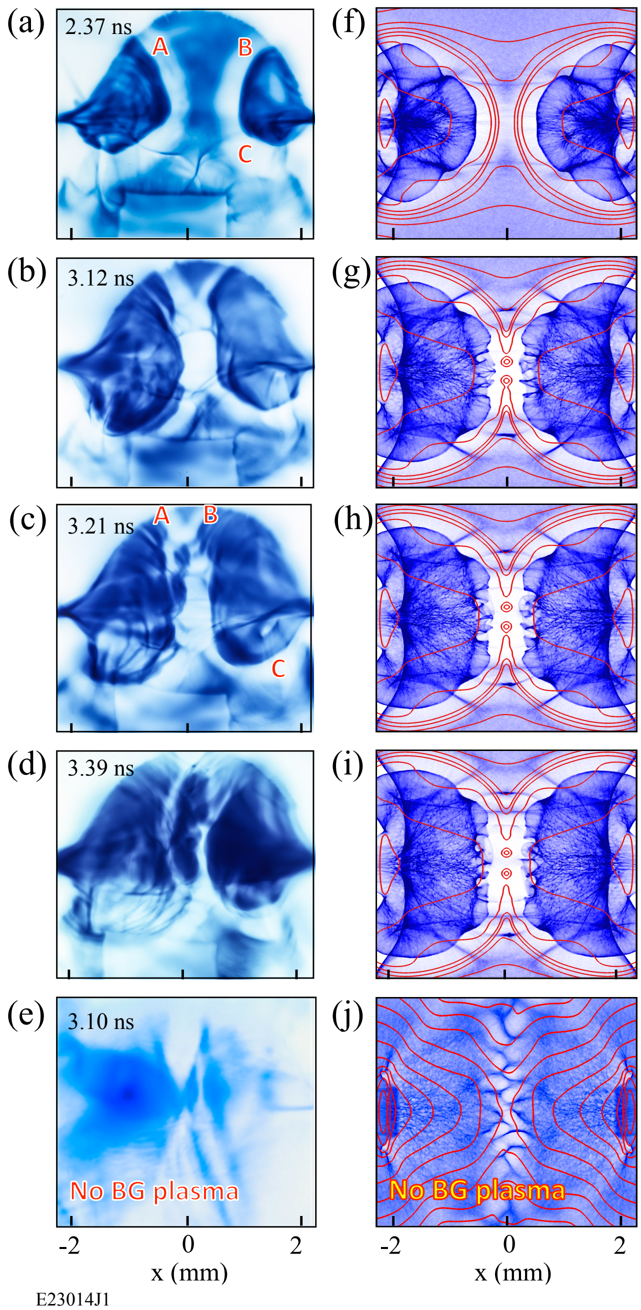

FIG. 2. (Color online). Proton radiographic images of the magnetic field evolution. The ablator targets are situated at the left and right borders of each frame. Dark areas correspond to high proton fluence. The series illustrates four stages in the magnetic field evolution: (a) formation of magnetic "ribbons" and the sweeping up of magnetic field, (b) magnetic ribbon collision, (c) reconnection, and (d) magnetic field annihilation. Frame (e) shows a proton radiography image without the background (BG) plasma. The time stamps on each frame show the time when the proton beam fired relative to the drive beams. The horizontal and vertical scales are the same. Results of simulated proton radiography at the corresponding times are shown in the right column, with overlaid magnetic field lines (red).

Figure 2c shows the magnetic field at a late nonlinear phase of reconnection, demonstrating a clear evolution in the topology of the current sheet. The plasma elements that were previously connected by the magnetic field (e.g., B and C) are now disconnected. Conversely, plasma elements that were previously disconnected (e.g., A and B) are now connected by the newly formed outflow magnetic field (V-shaped ribbons at the top and the bottom parts of the merged area) that disconnects from the central part of the current sheath and starts moving away. Furthermore, a small number of cellular structures appear, spanning the width of the current sheet. These structures can be plausibly interpreted as magnetic islands or plasmoid structures growing inside the current sheet.

Finally, Fig. 2d shows the disruption of the current sheet and annihilation of the magnetic fields, as the protons are no longer defocused from the sheet. The beginnings of this process may be reflected in the two dark blobs at the top of the current sheet in Fig. 2 (c). The annihilation (and indeed the entire evolution of the ribbons) occurs on a significantly faster time scale than the resistive diffusion (~ 10 ns) through the smallest plasma structures ($\sim 100\ \mu$m), so neither the reconnection or disruption are due simply to resistive dissipation. (Here the magnetic diffusion coefficient $D_m = \eta/\mu_0$ was evaluated from the Spitzer resistivity η at $T_e = 200\,$eV, a baseline prediction from simulations with the radiation hydrodynamics code *DRACO* [18]).

The right column of Fig. 2 shows results of accompanying particle-in-cell (PIC) simulations, which agree with the experiment on a number of features of the colliding ribbons. The 2-D simulations, with the invariant direction parallel to the MIFEDS currents, were conducted with the code *PSC* [19, 20] to help with both design and analysis of the experiments. The code solves the full relativistic, electromagnetic Vlasov-Maxwell system and includes a collision operator implementing Fokker-Planck collisions. The simulations provide an end-to-end model of the experiments, starting from vacuum magnetic field and followed by plasma formation, which is modeled with particle source terms set to obtain profiles similar to that provided by the radiation hydrodynamics code *DRACO* [18]. *DRACO* predicts plasma ablation densities near 6×10^{26} m^{-3} and background plasma densities near 2×10^{24} m^{-3}. Time is calibrated between simulation and experiment by matching the location of the ribbons at 2.37 ns; this corresponds to a sound speed of 1.8×10^5 m/s, which is, in fact, quite close to nominal *DRACO* predictions of 2×10^5 m/s. The magnetic fields were initialized as the vacuum fields from the two conductors. Synthetic proton radiographic images are obtained using a proton ray-tracing model. Magnetic field lines are shown as red curves, along with simulated proton fluence (blue) for direct comparison. More-detailed results of these simulations will be reported separately.

The simulations show similar formation and collision of magnetized ribbons, stagnation of the flows, and formation of an extended reconnection layer, which saturates at a width comparable to the ion skin depth. We find excellent agreement and reproduction of the formation of a caustic proton focusing feature on the back side of each ribbon. This feature is tracked in both experiment and simulation with excellent agreement and is shown in Fig. 3. The initial inflow speed, based on half the rate of change of the ribbon separation, is approximately 1×10^6 m/s. The collision velocity decreases as the ribbons collide and eventually stagnates for $t > 3$ ns.

The reconnection in the simulation occurs in a very fast burst, yielding the magnetic islands already growing and visible in the simulations at 3.12 ns. The peak electric field in the simulations, near 1.5×10^7 V/m, are comparable to "fastest-possible" reconnection rates inferred from reconnection inflows $v_{ribbon} = 1 \times 10^6$ m/s and B fields of order 25 T. Even accounting for flux pileup [19], the simulated reconnection rates are extremely fast, close to 100% of the local Alfvènic rate $B_* V_{A*}$, calculated based on the compressed magnetic fields and the plasma density in the current sheet. We find that the high compressibility of the current sheet, due to the super-sonic inflows, drives this reconnection rate, albeit transiently, which is significantly beyond what can be expected in steady state reconnection.

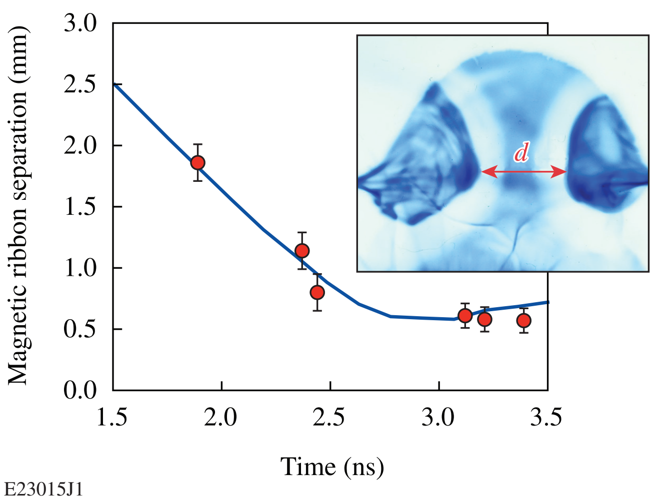

FIG. 3. (Color online). Measured time dependance of the separation d between the outer caustic boundaries of the magnetic ribbons (data points) compared with particle-in-cell (PIC) simulations (curve) showing inflow and stagnation of the flows.

The reconnection phase is followed by a complete magnetic annihilation, a point not observed in the simulations. In the simulated proton radiograph, the overall structure of the current sheet persists *after the reconnection* for some time. This is due primarily to the persistence of the magnetic islands in the current sheet, which formed due to reconnection but which have nowhere to go. In contrast, by 3.39 ns in the experimental data, there is a disruption of this current sheet structure, such that protons are no longer deflected at all. It is likely that 3-D effects not captured in the simulations are important for the fast disruption. Magnetic islands are special structures in 2-D, and could exhibit new dynamics in 3-D which allow complete disruption of the sheet current.

A final comment on the role of the background plasma is important. We find that the background plasma threaded by magnetic field is crucial to the formation of magnetized ribbons and subsequent reconnection. Embedding magnetic field into plasma is not trivial, since high-temperature, high-beta plasmas tend to expel magnetic fields. In previous HED laser-driven reconnection experiments [4, 5], the magnetic field was self-generated through the $\nabla n \times \nabla T$ effect so threading the plasma with magnetic field was automatic. In the present experiments, most of the flux threading occurs by the background plasma through parallel streaming from the source into the interaction region along the magnetic field lines.

Figures 2(e, j) show a proton radiography image (e) and associated simulation (j) where no background plasma is included. The most prominent features of the background plasma shots, namely the two strong-field ribbons and the topological changes in the ribbons geometry, indicating the reconnection, are totally absent. Overall, the images look very similar to that with no magnetic field [21]. The simulation show that the reason for this is that the majority of the magnetic flux is almost immediately lost from the gap, because it does not initially thread any plasma and so is free to instantly reconfigure as the two plumes begin to expand off the two surfaces.

In summary, magnetic reconnection of externally magnetized, colliding plumes of HED plasma has been demonstrated for the first time. The experimental results and numerical simulations show the formation and collision of magnetic ribbons, pile-up of the magnetic flux, and reconnection of the magnetic field. The reconnection is fast, with a transient reconnection rate comparable to the Alfvén reconnection rate. A feature crucial to the formation of magnetized ribbons and reconnection is the presence of the background plasma, the generation of which was externally controlled. The experimental results are generally in very good agreement with PIC simulations which model the experiments from end to end. Some features of the experiment, however, like the fast annihilation of the current sheet after the reconnection, are not displayed by the 2-D simulations and will be investigated in full-scale, 3-D simulations.

This work is supported by the U.S. Department of Energy under Contracts No. DE-SC0007168, DE-SC0008655, and DE-SC0006670, and the National Laser User Facility program. The particle-in-cell simulations were conducted on the Jaguar and Titan supercomputers through the Innovative and Novel Computational Impact on Theory and Experiment (INCITE) program. This research used resources of the Oak Ridge Leadership Computing Facility located in the Oak Ridge National Laboratory, which is supported by the Office of Science of the U.S. Department of Energy under Contract No. DE-AC05-00OR22725.

* gfik@lle.rochester.edu

[1] E. Priest and T. Forbes, *Magnetic Reconnection* (Cambridge University Press, 2000).
[2] D. Biskamp, *Magnetic Reconnection in Plasmas* (Cambridge University Press, 2000).
[3] M. Yamada, R. Kulsrud, and H. Ji, Rev. Mod. Phys. **82**, 603 (2010).
[4] P. M. Nilson, L. Willingale, M. C. Kaluza, C. Kamperidis, S. Minardi, M. S. Wei, P. Fernandes, M. Notley, S. Bandyopadhyay, M. Sherlock, R. J. Kingham, M. Tatarakis, Z. Najmudin, W. Rozmus, R. G. Evans, M. G. Haines, A. E. Dangor, and K. Krushelnick, Phys. Rev. Lett. **97**, 255001 (2006).
[5] C. K. Li, F. H. Seguin, J. A. Frenje, J. R. Rygg, R. D. Petrasso, R. P. J. Town, O. L. Landen, J. P. Knauer, and V. A. Smalyuk, Phys. Rev. Lett. **99**, 55001 (2007).
[6] P. M. Nilson, L. Willingale, M. C. Kaluza, C. Kamperidis, S. Minardi, M. S. Wei, P. Fernandes, M. Notley, S. Bandyopadhyay, M. Sherlock, R. J. Kingham, M. Tatarakis, Z. Najmudin, W. Rozmus, R. G. Evans, M. G. Haines, A. E. Dangor, and K. Krushelnick, Phys. Plasmas **15**, 2701 (2008).
[7] J. Zhong, Y. Li, X. Wang, J. Wang, Q. Dong, C. Xiao, S. Wang, X. Liu, L. Zhang, L. An, F. Wang, J. Zhu, Y. Gu, X. He, G. Zhao, and J. Zhang, Nature Physics **6**, 984 (2010).
[8] Q. Dong, S. Wang, Q. Lu, C. Huang, D. Yuan, X.Liu, X. Lin, H. Wei, J. Zhong, J. Shi, S. Jiang, Y. Ding, B. Jiang, K. Du, X. He, M. Y. Yu, C. S. Liu, S. Wang, Y. Tang, J. Zhu, G. Zhao, Z. Sheng, and J. Zhang, Phys. Rev. Lett. **108**, 215001 (2012).
[9] A. Bhattacharjee, Annu Rev Astron Astr **42**, 365 (2004).
[10] M. Opher, J. F. Drake, M. Swisdak, K. M. Schoeffler, J. D. Richardson, R. B. Decker, and G. Toth, Astrophysical Journal **734**, 71 (2011).
[11] J. F. Drake, M. Opher, M. Swisdak, and J. N. Chamoun, The Astrophysical Journal **709**, 963 (2010).
[12] J. Pétri and Y. Lyubarsky, Astronomy and Astrophysics **473**, 683 (2007).
[13] L. J. Waxer et al., Opt. Photonics News **16**, 30 (2005).
[14] O. V. Gotchev, J. P. Knauer, P. Y. Chang, N. W. Jang, M. J. Shoup, III, D. D. Meyerhofer, and R. Betti, Rev. Sci. Instrum. **80**, 043504 (2009).
[15] M. Borghesi, A. Schiavi, D. Campbell, M. Haines, O. Willi, A. MacKinnon, L. Gizzi, M. Galimberti, R. Clarke, and H. Ruhl, Plasma Phys. Contr F **43**, A267 (2001).
[16] M. Borghesi, A. J. Mackinnon, D. H. Campbell, D. G. Hicks, S. Kar, P. K. Patel, D. Price, L. Romagnani, A. Schiavi, and O. Willi, Phys. Rev. Lett. **92**, 55003 (2004).
[17] N. L. Kugland, P. Y. Chang, R. P. Drake, G. Fiksel, D. H. Froula, S. H. Glenzer, G. Gregori, M. Grosskopf, C. Huntington, M. Koenig, Y. Kuramitsu, C. Kuranz, M. C. Levy, E. Liang, D. Martinez, J. Meinecke, F. Miniati, T. Morita, A. Pelka, C. Plechaty, R. Presura, A. Ravasio, B. A. Remington, B. Reville, J. S. Ross, D. D. Ryutov, Y. Sakawa, A. Spitkovsky, H. Takabe, and H. S. Park, Phys. Plasmas **20**, 056313 (2013).
[18] P. B. Radha, V. N. Goncharov, T. J. B. Collins, J. A. Delettrez, Y. Elbaz, V. Y. Glebov, R. L. Keck, D. E. Keller, J. P. Knauer, J. A. Marozas, F. J. Marshall, P. W. McKenty, D. D. Meyerhofer, S. P. Regan, T. C. Sangster, D. Shvarts, S. Skupsky, Y. Srebro, R. P. J. Town, and C. Stoeckl, Phys. Plasmas **12**, 2702 (2005).
[19] W. Fox, A. Bhattacharjee, and K. Germaschewski, Phys. Rev. Lett. **106**, 215003 (2011).
[20] W. Fox, A. Bhattacharjee, and K. Germaschewski, Phys. Plasmas **19**, 056309 (2012).
[21] W. Fox, G. Fiksel, A. Bhattacharjee, P. Y. Chang, K. Germaschewski, S. X. Hu, and P. M. Nilson, Phys. Rev. Lett. **111**, 225002 (2013).